J Solid State Electrochem (2007) 11:1287–1294
DOI 10.1007/s10008-007-0288-2

ORIGINAL PAPER

Photoelectrochemical processes at interfaces of nanostructured TiO_2/carbon black composites studied by scanning photoelectrochemical microscopy

M. E. Rincón · M. E. Trujillo · J. Ávalos · N. Casillas

Received: 31 October 2006 / Revised: 16 January 2007 / Accepted: 6 February 2007 / Published online: 13 March 2007

Abstract The local photoelectrochemical response of TiO_2/carbon black photocatalysts was studied by means of scanning photoelectrochemical microscopy performed under UV illumination and external polarization. Catalysts obtained by sol-gel techniques showed a uniform response that improved under anodic polarization, in contrast to the non-uniform response of mixtures that show enhancement under cathodic polarization. To explain the differences in photoelectrochemical activity, we performed electrochemical and capacitive studies under dark condition, finding a larger positive shift in the rest potential of sol-gel composites plus evidence of Fermi-level pinning. We propose the last is related to the presence of carbon states with a strong acceptor character formed during the sol-gel synthesis. An energy band diagram of the composites were sketched based on the data obtained.

Keywords Titanium oxide · Carbon black · Photoelectrochemical · Mott–Schottky · Composites

Introduction

Nanocarbon particles have been used widely in the elaboration of catalysts as electrode supports to avoid catalysts agglomeration and to promote high surface area [1–5]. More recently, photocatalysts based on TiO_2/carbon black (CB) have been the subject of various studies, given that carbon have been reported to cause the narrowing of the band gap in titanium dioxide films [6–14]. Although the most common method for preparing a carbon-doped TiO_2 film is by direct oxidation of the Ti metal in the flame of a burner [12–14], solution methods have also been successful in presenting the optical sensitization phenomenon [9–11].

The typical morphology of TiO_2/carbon black composites is complex, polycrystalline, anisotropic, and heterogeneous. Its optimization requires a closer look into the local photocurrent of the composite films. In situ scanning photoelectrochemical microscopy (PM) is a powerful technique for mapping in real time the photocurrent distribution at the electrode–electrolyte interface [15–17]. The technique is sensitive to the geometry of the systems under study, and roughness can influence the intensity and the distribution of the detected photocurrent [17]. Still, in this contribution, we probe its usefulness in extracting information from nanostructured TiO_2 sensitized with carbon blacks. Studies performed by scanning PM, complemented by the use of capacitive techniques, provided interesting insights in the local reactivity of chemically and physically dispersed TiO_2/CB composites, aiding to the understanding of the reported differences in optical properties and photocatalytic activities of these composites [10, 11], where the average response gave little information about the relevance of the dispersion phenomena and/or the chemical composition at the electrode surface. Consequently, the ultimate motivation of this contribution is to understand and, therefore, being able to control through optimized synthesis the local reactivity of chemically and physically dispersed TiO_2/CB composites.

M. E. Rincón (✉) · M. E. Trujillo
Centro de Investigación en Energía-Universidad Nacional Autónoma de México,
Apartado Postal 34, Temixco 62580 Morelos, Mexico
e-mail: merg@cie.unam.mx

J. Ávalos · N. Casillas
Departamento de Química, Universidad de Guadalajara,
Boulevard Marcelino García Barragán #1451,
Guadalajara 44430 Jalisco, Mexico

Experimental

Synthesis of TiO_2/carbon black photocatalysts

Nanometric TiO_2 was prepared by the sol-gel technique at low temperature (0 °C). Briefly, 2.8-ml $TiCl_4$ (Aldrich) was added (drop by drop) to 100-ml 1M HCl aqueous solution. Immediately after addition, the low pH was adjusted to a value of 3 with concentrated ammonia. After vigorous stirring for 24 h, precipitates were obtained by *sol* neutralization. These solids were washed abundantly with distilled water and dehydrated at 100 °C. For the case of TiO_2 with 10 wt% CB (supplied by Columbian Chemical, 123 m^2/g), a similar procedure was followed with the proper amount of CB dispersed as an ink before the addition of $TiCl_4$. The ink contained small amounts of propylenglycol and triton X-100 that were removed during the annealing of the precipitates. Photoelectrodes were prepared by placing the paste resulting from mixing the dried photocatalysts with minor amounts of X-triton and propylenglycol onto conductive glass substrates (Delta Technologies, 25×75×1.1 mm unpolished float glass, SiO_2 passivated/indium tin oxide coated one surface, R_S= 4–8 Ω). After further annealing at 450 °C for 1 h in air (films without CB) and N_2 (films with CB), the films' thickness was in the range of 7–13 μm. Fourier transform infrared (FTIR) analysis indicated that most of the organic components were removed after annealing but hydroxyl groups still persisted on the TiO_2 surface [11]. Electrodes based on mixtures of CB and commercial TiO_2 (Spectrum, 50 m^2/g) were prepared in a similar manner and compared to the sol-gel composite. The crystalline grain size of these powders have been reported [10, 11] and corresponded to $TiO_{2sol\text{-}gel}$ ~ 5 nm < $[TiO_2/CB]_{sol\text{-}gel}$ ~ 8 nm < $[TiO_{2com}/CB]_{mixture}$ ~ 30 nm < $[TiO_{2com}]$ ~ 35 nm.

Photoelectrodes characterization

Scanning PM studies were performed with a home-built apparatus in 0.05-M H_2SO_4 solutions saturated with N_2. Figure 1 shows the experimental setup and the characteristics of the system used. A He–Cd laser beam model omnicrome 56 from Melles Griot, with a wavelength of λ= 351 nm and a power of 4.2 to 10 mW, was used as an illuminating source. The laser beam was focused into a multimodal optical fiber 50/125 using a coupler at the backside of the optical fiber sensor model F-916 from Newport. The fiber optic probe was vertically held on an *x*–*y*–*z* translation stage model MM4005 from Newport and immersed in 0.05-M H_2SO_4 solution. A potentiostat was used to control the potential of the screen-printed film electrodes during illumination. A three-electrode electrochemical cell configuration was completed by using a saturated calomel electrode (SCE) as reference and a Pt counter electrode. The photocurrent measured from the screen-printed film electrodes was acquired as a function of the *x*–*y* position along the scan, and as long as the distance of the optical fiber to the electrode surface was maintained well above the roughness of the substrate (i.e., millimeters vs. micrometers), the photocurrent scan was sensitive only to the presence of photoactive material.

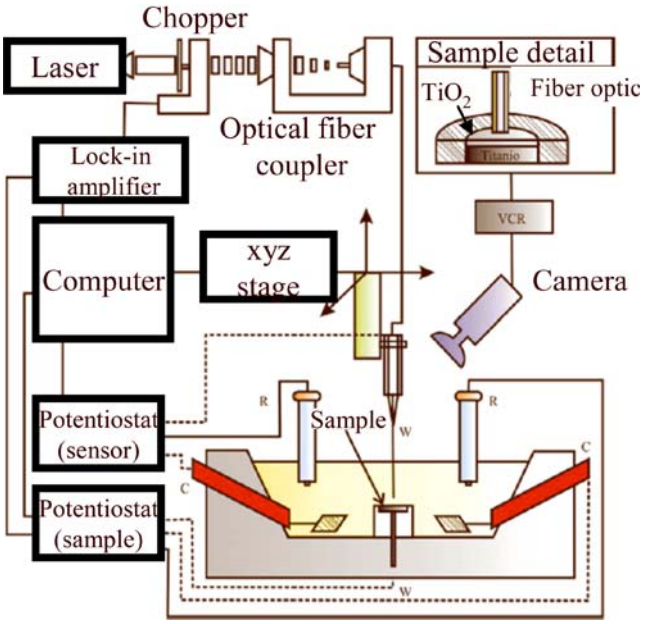

Fig. 1 Experimental setup of the scanning photoelectrochemical microscope system used to obtain the local photocurrent activity of composite electrodes based on TiO_2/carbon blacks. See the text for its description

Cyclic voltammetry experiments and electrochemical capacitance measurements were carried out in a single compartment three-electrode glass cell, with Hg/Hg_2SO_4 as the reference electrode and Pt wire as the counter electrode. The screen-printed film working electrode was mounted parallel to the reference electrode and had a 1-cm^2 exposed geometric area. Electrochemical measurements were obtained with a Solartron system, where the ac impedance measurements (averaged over 10 cycles) were carried out with a 10-mV (rms) amplitude, at fixed frequency in the potential range of −1.0 to 1.0 V vs SCE.

Results

Photoelectrochemical characterization

The PM data of sol-gel TiO_2 photoelectrodes obtained as a function of external polarization are shown in Fig. 2. The images are taken at applied potentials (*U*) more positive (anodic polarization) or more negative (cathodic polarization) than the rest potential measured under dark condition

and labeled V_{oc}: Fig. 2a, $U = V_{oc}$=0.0 V vs SCE; Fig. 2b, U= −500 mV vs V_{oc}; Fig. 2c, U=500 mV vs V_{oc}. From these images, it is clear that a significant increase in photocurrent takes place under positive bias, while just a minor increase in photocurrent appears at negative polarizations.

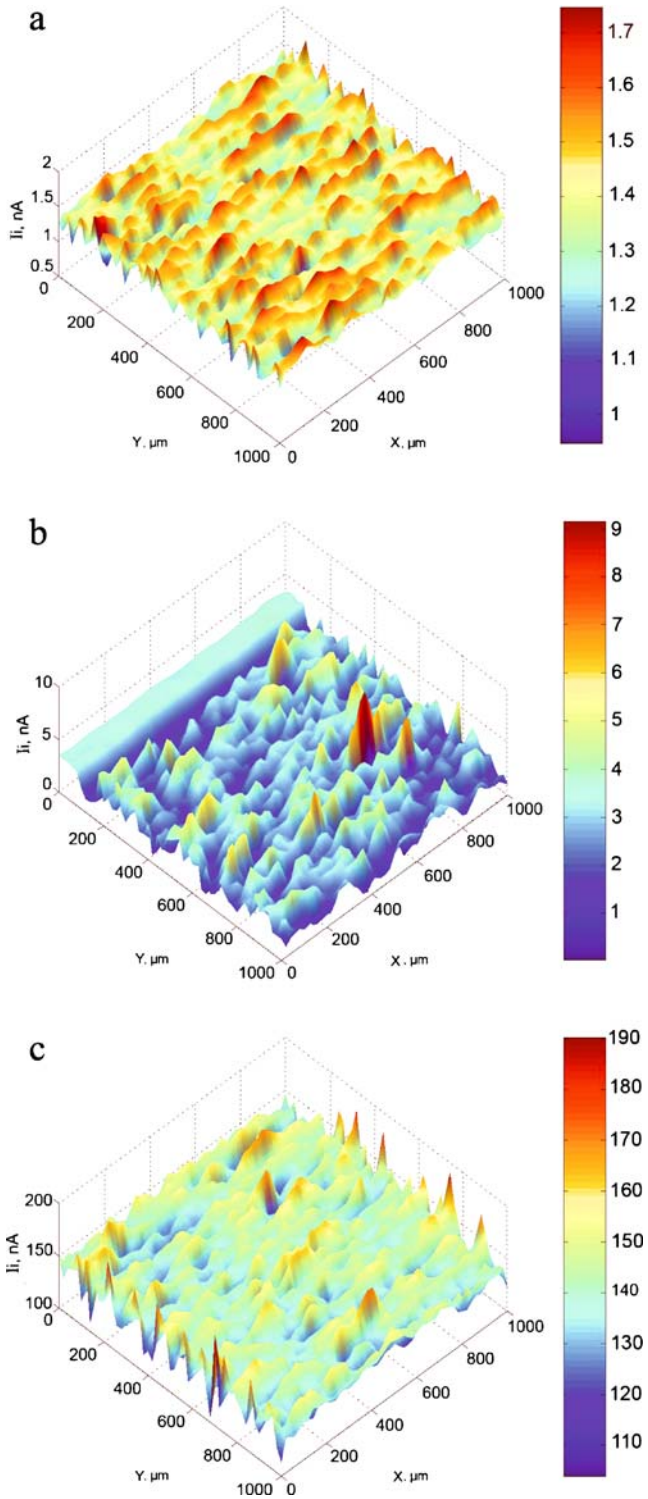

Fig. 2 Scanning photoelectrochemical microscopy data of sol-gel TiO_2 photoelectrodes obtained as a function of external polarization: **a** images at rest potential (V_{oc}=0.0 V vs SCE), **b** at cathodic polarization (−500 mV vs V_{oc}), **c** at anodic polarization (500 mV vs V_{oc}). Scan rate of 200 µm/s. Data obtained at ambient conditions in 0.1 N H_2SO_4

For sol-gel TiO_2/CB composite electrodes, the PM images are shown in Fig. 3, where we compared the effect of surface activation and polarization. Carbon materials usually require surface activation to remove adsorbed species and to passivate the most reactive sites that can act as recombination sites; in our experiments, this was performed by cycling between −1 V vs SCE to +0.1 V vs SCE. A significant increase in photocurrent was observed after surface activation (Fig. 3a vs b), but no differences were found relative to polarization (Fig. 3b taken at V_{oc} vs c taken at +0.6 V vs V_{oc}), in clear contrast to the potential dependence found on sol-gel TiO_2 electrodes. For electrodes based on commercial TiO_2 ($TiO_{2\ com}$) and mixtures of $TiO_{2\ com}$ and CB $(TiO_{2\ com}/CB)_{mixture}$ (Fig. 4), no major changes were observed under anodic polarization, but a notorious increase in photocurrent was observed at negative bias with the scale changing from 0.45 nA at V_{oc} to 400 nA at −0.3 V vs V_{oc}. Moreover, the photocurrent in these electrodes was found to be higher than that in sol-gel composites and also more sensible to the dilution effect caused by the presence of carbon blacks. Both electrode mixtures and sol-gel composites had rest potentials (measured at dark condition) shifted to more positive values due to the presence of carbon blacks.

Electrochemical characterization

To select the potential range appropriate for Mott–Schottky (MS) modeling (i.e., a potential range with maximum capacitive current and minimum redox contribution), cyclic voltammograms were obtained in 0.1-M H_2SO_4 at scan rates of 10–100 mV/s. Similar geometric area (1 cm^2) and measurement conditions were used in all the screen-printed electrodes. The results are shown in Fig. 5, where redox peaks at −0.5 V vs SSE and 0.1 V vs SSE are notorious in the I–V curves of the oxides and composites obtained by the sol-gel route (Fig. 5a), in contrast to the dominant capacitive current of the commercial oxide and its mixtures with CB (Fig. 5b).

In ideal semiconductor/redox electrolyte interfaces, the presence of an energetic barrier in the semiconductor phase, originated by the equilibration of the electron Fermi level in the solid (E_F) and liquid phases (E_{redox}), can be approximated by the semiconductor depletion layer capacitance C_{sc} and the MS equation expressed as [18]

$$1/C_{sc}^2 = (2/\varepsilon\varepsilon_o N_D)(\Delta\Phi sc - kT/e); \quad (1)$$

here N_D is the donor concentration in cm^{-3}, e is the charge of the electron, k is the Boltzman constant, T is the

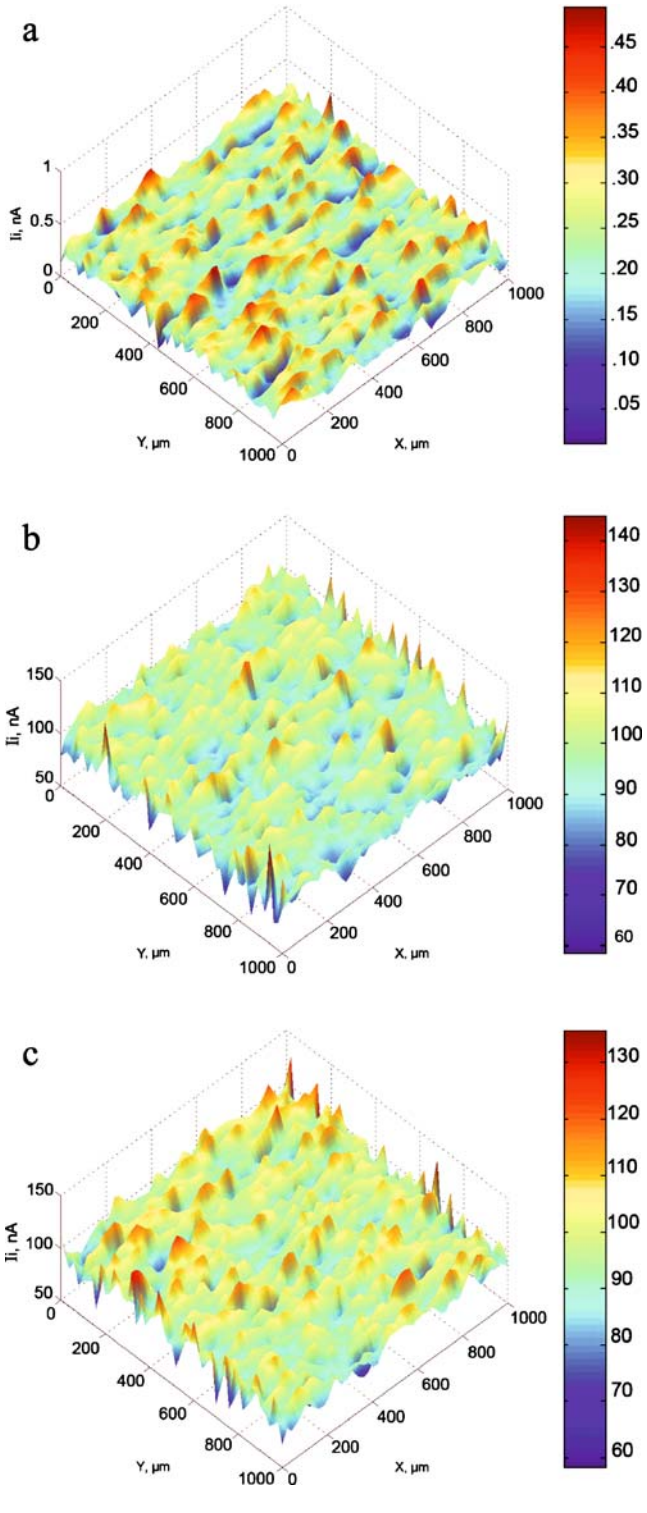

Fig. 3 Scanning photoelectrochemical microscopy data of sol-gel TiO_2/carbon black composite electrodes containing 10 wt% carbon black: **a** photocurrent obtained at rest potential (V_{oc}=0.1 V vs SCE), **b**–**c** images of activated surfaces, **b** at rest potential, **c** under anodic polarization of +0.6 V vs V_{oc}. Activation was performed electrochemically by cycling the electrodes between −1 and +0.1 V vs SCE. Data obtained at ambient conditions in 0.1 N H_2SO_4 at 200 μm/s scan rate

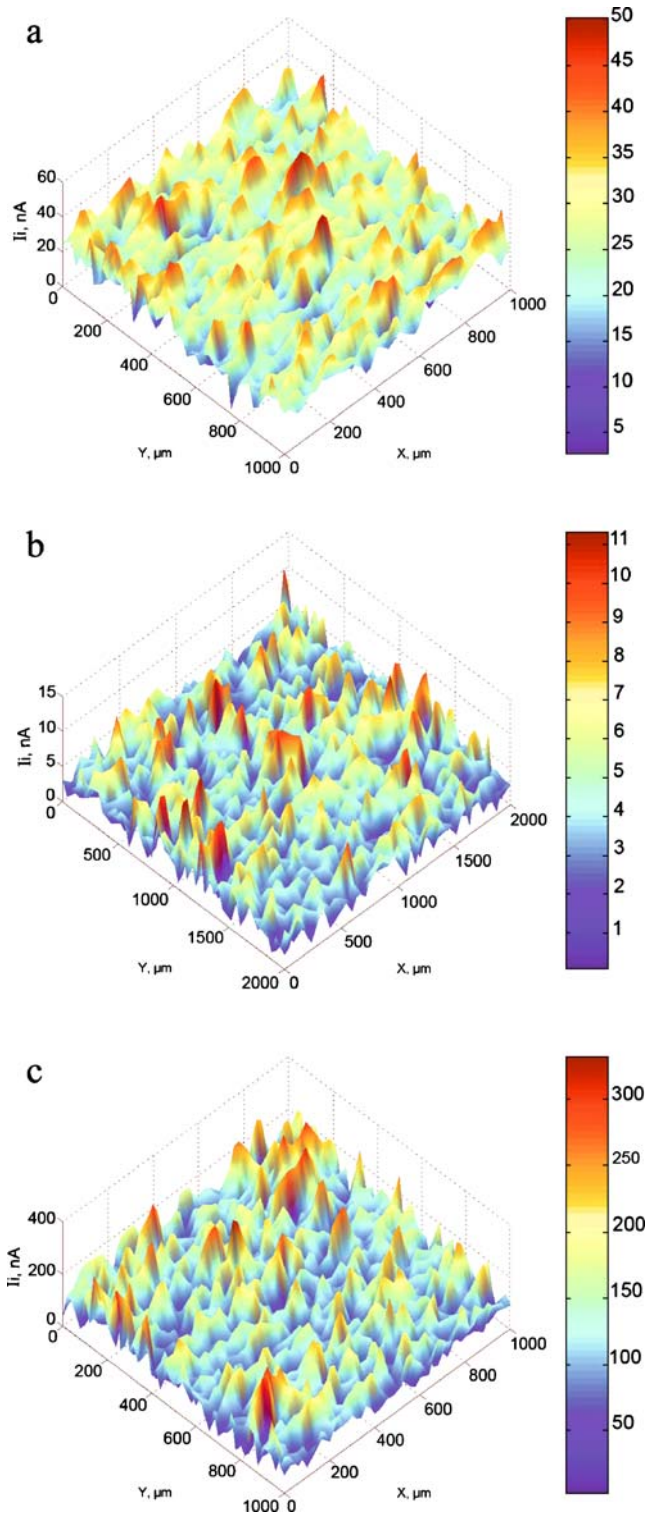

Fig. 4 Scanning photoelectrochemical microscopy data of electrodes based on commercial TiO_2 and mixtures of commercial TiO_2 and 10 wt% carbon blacks: **a** image of the oxide at 0.25 V vs V_{oc} (V_{oc}= 0.05 V vs SCE), **b**–**c** images of activated mixtures, **b** at V_{oc}=0.3 V vs SCE, **c** under cathodic polarization of −0.3 V vs V_{oc}. Data obtained at ambient conditions in 0.1 N H_2SO_4 at 200 μm/s scan rate

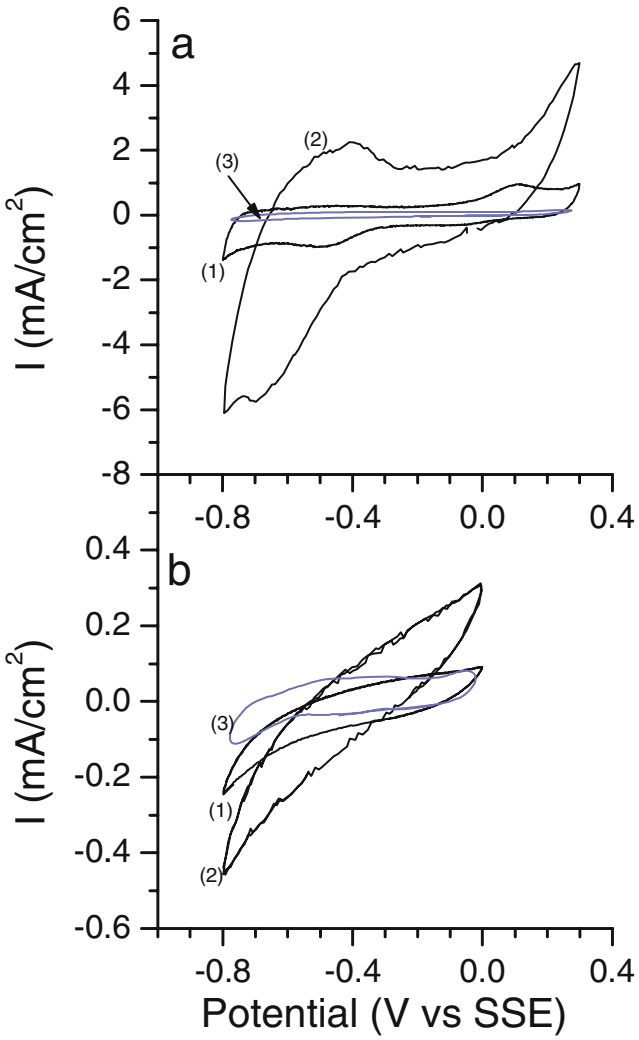

Fig. 5 Cyclic voltammograms of nanoporous TiO_2-composite electrodes based on 10 wt% carbon blacks in 0.1 M H_2SO_4 at various scan rates (1–10, 2–100, and 3–100 mV/s). **a** Electrodes based on sol-gel oxides and composites; **b** electrodes based on commercial oxide and mixtures. Label *3* marks the I–V curves of the oxide matrices

temperature, and ε and ε_o are the dielectric constant and vacuum permittivity of the semiconductor, respectively. $\Delta\Phi$sc represents the potential drop into the semiconductor and $\Delta\Phi$sc=0 (no potential drop within the semiconductor) corresponds to the flat band condition. In terms of the electrode potential U, $\Delta\Phi sc = U - U_{fb}$; hence, U_{fb} can be obtained from the intersection with the potential axis of the linear plot of C^{-2} vs U, while the slope m is inversely proportional to N_D.

The MS plots of the electrodes based on sol-gel materials are presented in Fig. 6; here, the nanometric sol-gel oxide (Fig. 6a) shows the pattern expected for n-type semiconductors, while the sol-gel composites (Fig. 6b) apparently shows both inversion (*negative* slope) and depletion zones (*positive* slope) in a narrow potential interval. In these electrodes, CBs shift the flat band potential of the oxide by almost 300 mV, from 0.1 to 0.4 V vs the normal hydrogen electrode (NHE), which is larger than the shift observed in carbon-modified titanium dioxide [8], where the flat band potential moves from −520 mV to −0.39 V vs NHE. For electrodes based on commercial oxides, Fig. 7 shows similar MS plots for oxides (Fig. 7a) and mixtures (Fig. 7b), with m and U_{fb} barely changing by the addition of carbon blacks. The value of U_{fb}=100 mV vs NHE is close to the reported value of TiO_2 films with relatively low donor concentration [19].

The frequency dependence of U_{fb} and m values obtained from Figs. 6 and 7 is summarized in Table 1, where we can see that U_{fb} barely changes with frequency but m clearly decreases at higher frequencies. In ideal semiconductor/electrolyte interfaces, this dependency is not accounted for and explains why the donor concentration obtained by using the geometric area of the electrode is 3–4 orders of magnitude above the expected donor concentration of passive films [18]. It is apparent that the absolute values of C and m can not be quantitatively associated to C_{sc} or N_D

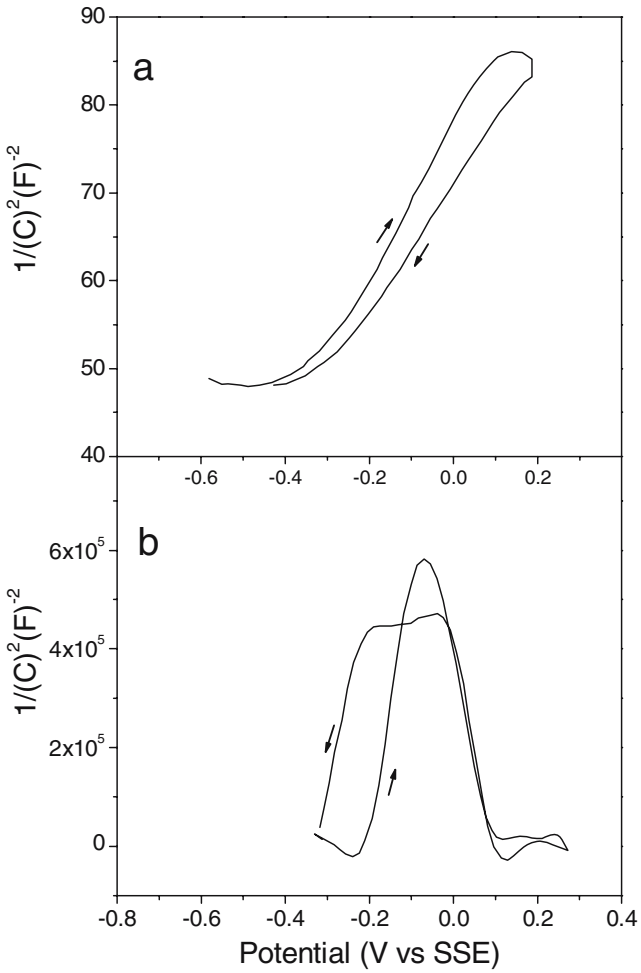

Fig. 6 Mott–Shottky diagrams of sol-gel oxides (**a**) and sol-gel composites (**b**) obtained at 100 Hz and 10 mV/s scan rate in 0.1 M H2SO4. The oxide shows the pattern expected for n-type semiconductors, while the sol-gel composites apparently shows both the depletion and the inversion zones in a narrow potential interval

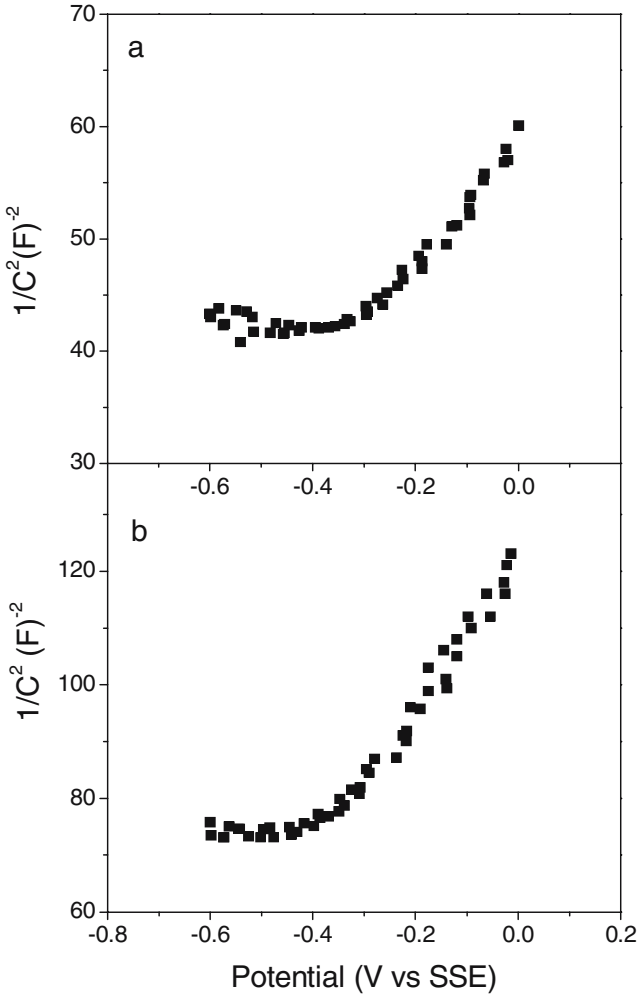

Fig. 7 MS plots for electrodes based on commercial oxides, where the n-type nature of the oxide (**a**) and its flat band potential barely change by the addition of carbon blacks (**b**). Data obtained at 10 Hz and 10 mV/s scan rate in 0.1 M H_2SO_4

without correcting for the roughness factor (i.e., active surface area ≫ geometric area), the contribution of the double layer capacitor C_H, and/or the contribution of the pseudofaradic reactions observed on the cyclic voltammograms. The mild frequency dependence of the flat band, on the other hand, follows the trend expected for the presence of a large donor density, where the potential drop along the double layer capacitor causes a positive shift [18]:

$$U_{fb} \sim U_0 - kTe + \varepsilon\varepsilon_o e N_D / 2C_H^2 \quad (2)$$

Here, U_o is the intersection of the MS plot with the potential axis. The required correction in the U_{fb} value remains negligible as long as the dielectric constant ε and donor density N_D are small. For the composites studied, the positive shift appears at low frequencies due to the contribution of surface states and could be as high as 500 mV. It corresponds to N_D in the order of 1.9×10^{20} cm^{-3}, assuming that C_H=20 μF/cm^2 and ε (TiO_2)=173 [19].

Discussion

Sol-gel composites and ex situ mixtures of sol-gel oxides and CB (not shown) are electrochemically active in acid media. They show redox peaks similar to the one shown in Fig. 5a, where the electrochemical activity is likely a combination of good electronic conductivity (better dispersion of carbon blacks) and the synergism between the hydroxylated oxide and the oxygenated groups on the carbon surface. These redox peaks fade away during electrochemical activation and are absent in mixtures of CB and commercial TiO_2.

Interestingly, the superior dark current of sol-gel materials does not manifest as PM images with superior local photocurrent. A priori, one would expect that the enhanced dispersion of sol-gel composites brings a substantial increase in the semiconductor/electrolyte interface aiding to charge transfer in both dark and illuminated conditions. The fact that this does not occur suggest a complex role for the intimate oxide/CB interface of sol-gel materials. The scanning PM provides information on the local photoelectrochemical activity due to water oxidation/reduction reactions driven by photogenerated electron/hole pairs. It is sensible to the dispersion of the photoactive material and/or to electron/hole recombination caused by poor electron transfer kinetics and the abundance of surface states. Because PM images agree well with the expected distribution of the photoactive material, giving near-homogeneous values in sol-gel composites where the oxide grows on top of the CB, while bright and dark zones are typical of

Table 1 Flat band potentials U_{fb} and m values at selected frequencies

Material	U_{fb} vs NHE (V)	Frequency (Hz)	m[a] ($F^{-2}V^{-1}$)
$TiO_{2\ sol\text{-}gel}$	−0.1:0.2	1	3,000
		10	600
		100	100
$(TiO_2/CB)_{sol\text{-}gel}$	0.4:0.5	1	6×10^6
		10	
		400	
$TiO_{2\ coml}$	0.1	1	600
		10	100
		100	–
$TiO_{2\ com}$ + CB	0.1	1	700
		10	100
		100	–

[a] Slope of the line intersecting the U-axis in a C^{-2} vs U graph

mixtures, the likely presence of electron/hole recombination is further discussed.

The sensitivity of PM images to small potential bias gives information on the recombination phenomena. Sol-gel TiO_2 photoelectrodes obtained as a function of external polarization (Fig. 2) show the behavior expected in n-type nanostructured electrodes (photoanode under illumination) where the abundance of surface states propiciates near flat-band condition, and small positive potential bias helps to overcomes hole's recombination under illumination. On the contrary, sol-gel composites do not show any preferences relative to polarization (Fig. 3b and c) that seems to agree with the maximum observed in the MS plot. Here, an inversion zone or a pseudocapacitor assigned to faradic events contribute at large positive bias. For $TiO_{2\ com}$ and $TiO_{2\ com}$/CB, no major changes in PM images were observed under anodic polarization but a notorious increase in photocurrent was evident at negative bias. That suggests the presence of energy barriers for the reduction reaction instead of recombination problems related to the lack of a well-defined depletion zone that is not supported by MS data. Energy barriers for hydrogen or peroxide production appear when the potential of the conduction band is not negative enough.

In regard to the information extracted from the simplified MS equation, this is based on the analysis of the differential capacitance measurements of the semiconductor/electrolyte junction in semiconductors that are not heavily doped or have an abundance of surface states. That is hardly the description of the sol-gel materials, and we proposed that the inversion and depletion zones observed in sol-gel composites reflect the contribution of the redox reaction at 0.1 V vs SSE, explaining also the large hysteresis of this material. Because ex situ mixtures of sol-gel oxides and carbon blacks also show the inversion zone (or negative slope), but not the mixtures based on commercial oxides, the functionality of the sol-gel oxide plays an important role in promoting this faradic events, most likely by contributing to the abundance of surface states and Fermi level pinning.

Energy band diagrams

The energy diagrams presented on Fig. 8 took into account the electrochemical and PM characterizations. The flat band potentials were drawn according to the MS plots because of the small frequency dependence observed in U_{fb} values. The bending on the bands reflects the bias-dependence found on the PM data. Notice the bands of the sol-gel oxides drawn flat, as it is under anodic polarization where the enhancement on photocurrent was observed (i.e., at positive bias charge separation is promoted and oxidation processes at the interface are facilitated). The energy bands

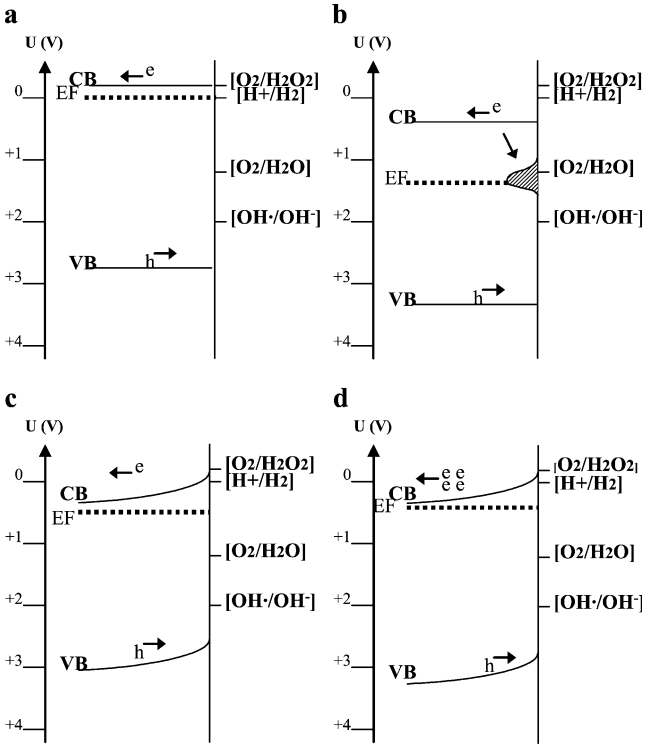

Fig. 8 Energy band diagrams of the electrodes studied. **a** TiO_2sol-gel, **b** (TiO_2/CB)sol-gel, **c** TiO_2com, **d** (TiO_2 com + CB) mixture. Flat band potentials are drawn according to Table 1. The bands of the sol-gel oxides and composites are drawn flat, while carbon states pinned the Fermi level close to the middle of the band gap in sol-gel composites. For commercial oxides and its mixtures, the bands are bent and the peroxide route is barely accessible

of sol-gel composites were drawn flat also but at more positive potentials, as carbon states pinned the Fermi level close to the middle of the band gap. The unpinning of the bands (i.e., the switch from band pinning to Fermi level pinning) causes the insensitivity of the activated surfaces to external polarizations, as most of the potential drop occurs inside the double layer. We proposed that after surface activation the enhancement in photocurrent is observed because many of the reactive recombination sites become passive. In sol-gel composites, and perhaps due to the intimate oxide/carbon bond, carbon might act as a sink for the photogenerated electrons that can not be consumed by the peroxide or hydrogen routes avoiding hole recombination. The presence of carbon states in the middle of the oxide band gap also explains the optical sensitization [10] and the improved long-time photocatalytic activity found on these materials [11]. For commercial oxides and its mixtures, where the enhancement in photocurrent is observed under cathodic polarization, the bands are drawn with enough curvature to exemplify that a well-defined barrier for electrons inhibits the peroxide route. In physical mixtures, carbon blacks do not fulfil the role of electron sequesters, and this leads to the accumulation of photo-generated electrons followed by holes annihilation.

Conclusion

We report the photoelectrochemical activity of TiO_2/carbon black photocatalysts. Scanning PM studies were performed under external polarization in acid media with film electrodes illuminated with UV light. Without external polarization, small photocurrent intensities were observed for nanostructured carbon-doped TiO_2 films and photoelectrodes based on ex situ mixtures of commercial TiO_2 and carbon blacks. Enhancement on photocurrent occurs after the surface activation on both composites, although the preference for anodic polarization shown by the sol-gel oxide is erased on electrodes based on sol-gel composites, while cathodic polarization is still required on the mixtures. Cyclic voltammetry and capacitance studies performed under dark condition complemented the PM data and allow us to draw schematic energy band diagrams explaining the structure-dependent role of carbon blacks, which creates acceptor states on sol-gel composites. These data are relevant to the design and application of photocatalysts in electrochemically assisted photocatalysis and provide further insight into the properties of sol-gel TiO_2 sensitized by nanometric carbon blacks.

Acknowledgment We acknowledge the technical assistance of Rogelio Morán Elvira, as well as the funding provided by CONACYT-Mexico (fellowship for M. E. Trujillo), and UNAM-Mexico through the projects PUNTA and IN111106-3.

References

1. Hermann JM, Matos J, Disdier J, Guillard C, Laine J, Malato S, Blanco J (1999) Catal Today 54:255
2. Takeda N, Iwata N, Torimoto T, Yoneyama H (1998) J Catal 177:240
3. Torimoto T, Okawa Y, Takeda N, Yoneyama H (1997) J Photochem Photobiol A 103:153
4. Modestov A, Glezer V, Marjasin I, Lev O (1997) J Phys Chem B 101:4623
5. Araña J, Doña-Rodríguez JM, Tello Rendón E, Garriga i Cabo C, González-Díaz O, Herrera-Melián JA, Pérez Peña J, Colón G, Navío JA (2003) Appl Catal B 44:161
6. Li D, Haneda H (2003) J Photochem Photobiol A 160:203
7. Lettmann C, Hildenbrand K, Kisch H, Macyk W, Maier WF (2001) Appl Catal B 32:215
8. Sakthivel S, Kisch H (2003) Angew Chem Int Ed 42:4908
9. Khan SUM, Al-Shahry M, Ingler WB (2002) Science 297:2243
10. Rincón ME, Trujillo-Camacho ME, Cuentas-Gallegos AK (2005) Catal Today 107–108:606
11. Rincón ME, Trujillo-Camacho ME, Cuentas-Gallegos AK, Casillas N (2006) Appl Catal B 69:66
12. Fujishima A, Kohayakawa K, Honda K (1975) J Electrochem Soc 122:1487
13. Noworyta K, Augustynski (2004) J Electrochem Solid State Lett 7:E31–E33
14. Walsh DA, Fernández JL, Bard AJ (2006) J Electrochem Soc 153: E99–E103
15. Garfias-Mesias LF, Smyrl WH (1999) J Electrochem Soc 146:2495
16. Haram SK, Bard AJ (2001) J Phys Chem B 105:8192
17. Maffi S, Lenardi C, Bozzini B, Peraldo-Bicelli L (2002) Meas Sci Technol 13:1398
18. Di quarto F, Santamaria M (2004) Corros Eng Sci Technol 39:71
19. Rajeshwar K (2001) Fundamentals of semiconductor electrochemistry and photoelectrochemistry. In: Licht S (ed) Encyclopedia of electrochemistry, vol 6. Wiley–VCH, Weinheim, pp 3–53